Engineering of a Ge-Te-Se glass fibre evanescent wave spectroscopic (FEWS) mid-IR chemical sensor for the analysis of food and pharmaceutical products

Xin Jiang[1,2]* and Animesh Jha[1]

[1]*The Institute for Materials Research, Houldsworth Building, University of Leeds, LS2 9JT, United Kingdom*

[2]*Max-Planck-Institute for the Science of Light, Guenther-Scharowsky-Strasse 1/Bau 24, Erlangen 91058, Germany*

Abstract: Using an unclad multimode Ge-Te-Se based chalcogenide glass fibre, simple design robust fibre evanescent wave spectroscopic (FEWS) sensor is demonstrated. Methodologies adopted for material development and fiber drawing are discussed in the following steps: purification of raw materials for high spectral purity, fabrication of glass and fibre preform leading to fibre drawing. The fabricated fibre has a minimum loss of 1.4 dB/m at 4.2 μm, and less than 3 dB/m between 1.5 and 6.3 μm. The feasibility of using such a fibre for evanescent wave spectroscopic sensing has been verified by using the finite-element (FE) computation technique. Supported optical modes as well as corresponding penetration depths of evanescent fields from different modes are discussed. Based on the FE computation, a FEWS sensor consisting of a 40 cm Ge-Te-Se fibre, coupled with a Fourier transform infrared (FTIR) spectrometer and a liquid nitrogen cooled Mercury-Cadmium-Tellurium (MCT) detector, is demonstrated. The active length along this fibre employed for sensing is 3 cm. Based on FEWS design, the fabricated fibre sensor was used for the analysis of chemicals, namely the acetone, ethanol, methanol, tocopherol (vitamin E), ascorbic acid (vitamin C), fresh orange and lemon juice.

Keywords: Chalcogenide glass fibre, Chemical sensing, FTIR, FEWS

1. Introduction

Visible and near infrared (IR) optical fibre sensing for analyzing the presence of chemical species in an environment is becoming an important tool for food, pharmaceutical and petro-chemical manufacturing. The sensor is an essential tool for product quality control. For determining concentrations in ppm to sub-ppm range, it is important to perform measurements in the mid-infrared (mid-IR) spectral region where molecules have large fundamental vibration bands which

are 10^3-10^5 times larger than their weaker harmonics in the visible and near infrared (NIR) regions [1]. However, for accessing mid-IR the standard silica fibres are opaque beyond 2 µm due to their core-clad structure design. One exception is a simplified hollow core fibre structure demonstrated recently [2]. Knight et al explained the principle of anti-resonant reflecting optical waveguide (ARROW) using silica materials and demonstrated a discontinuous transmission window between 3 and 4 µm. The current limit is the difficulties in using other infrared glasses for fabricating such ARROW fibres, for which we believe the transmission and spectroscopic properties may be further improved, provided the glass material used exhibits the extended infrared transmission beyond the current range of solid-core silica. Unlike ARROW design, solid core-clad mid-infrared fibres using heavy metal oxide and chalcogenide glasses have demonstrated the usefulness in terms of accessing the mid-IR for chemical/biological sensing [1, 3-8]. Using such solid core fibre structures, a number of chemical species (benzene (C_6H_6) [1], toluene (C_7H_8) [1], sulfuric acid (H_2SO_4) [3], methanol (CH_3OH) [4], methane (CH_4) [4], ethanol (C_2H_5OH) [5], acetone ((CH_3)$_2CO$) [6-8] were analyzed and reported. In these analysis, the molecular vibrations e.g. O-H, C-H, C≡C, C=O and S-H in the 2 to 16 µm [9, 10-13] were targeted.

Amongst the optical fibre sensor designs, fibre evanescent wave spectroscopic (FEWS) sensors were extensively studied [3, 14-16]. In a FEWS two different geometrical designs were researched for sensing chemical species using silica and non-silica fibres. In the first type of design a standard core-clad structure fibre with small numerical aperture (<0.15) is used for allowing the modes to leak into the cladding through which the leaky waves are absorbed by the chemical species, present in the environment. The drop in the intensity is then related with the concentration which is determined by using the Lambert-Beer's law. [5, 7, 12, 15]. In an alternative design, the cladding layer is removed and the core acts as a guiding region in the presence of medium to be analyzed. For the unclad fibre or waveguide design, the surrounding medium must be of lower index than the core glass [3, 6, 8, 9, 11-16]. Further enhancement in the concentration sensitivity in unclad fibre/waveguide design was demonstrated using tapered and nano-fibres [17-21], allowing sub-ppm concentration analysis. However, for high sensitivity (10^3-10^5) and signal-to-noise ratio, the spectral range between 2 and 16 µm appears ideal for a range of spectroscopic characterization

using a suitable transparent medium, which must be a non-silica host due to the strong multiphonon absorption in the core-clad silica and ARROW structures. This implies the use of candidate fibres such heavy metal oxide, fluoride and chalcogenide fibres, amongst which the chalcogenide fibres have the most extended IR absorption and multiphonon edges due to large reduced mass and weak interatomic force constant. As in the history of the development of silica fibres, it is essential that such mid-IR fibres must be spectroscopically unobscured with impurity bands. The chalcogenide materials often have strong impurity bands and these must be minimized. In the context of impurity control, this paper discusses the methodology for minimizing the impurities in designed Ge-Te-Se fibres.

Based on the extended multiphonon absorption in chalcogenide materials and advantages of unclad waveguide geometry in FEWS design, in this paper, an unclad, multimode Ge-Te-Se based chalcogenide glass fibre sensor is demonstrated for chemical analysis in the 3-6 μm window. Methods of glass and preform fabrication leading to fibre drawing is described. The fibre loss measurements in the unclad geometry for FEWS is also described for the above spectroscopic window using a fibre coupler and Fourier transform infrared spectrophotometer. The feasibility of using such an unclad fibre for FEWS sensing is also verified by finite-element (FE) calculations, supporting the optical modes penetrating into the evanescent field in a 3 cm long sensing length. Finally, our target analyte such as acetone, ethanol, methanol, tocopherol (vitamin E) and ascorbic acid (vitamin C), are characterized by using the Lambert-Beers law in the FEWS design and the results are reported.

2. Material development and fibre drawing

2.1 Raw material purification glass fabrication and

The fabrication of low-loss chalcogenide glass fibres and waveguides has remained challenging, mainly due to the following two reasons: the propensity of absorption of impurities in raw materials and high vapor pressures of constituent elements at temperatures, which result in sub-stoichiometric (e.g. metal or metalloid ions to chalcogenide ion) compounds (GeS_{2-x}). Such an

intrinsic origin for sub-stoichiometry then tends to contribute to the background loss at short wavelengths, leading to electronic edge. It is also known that chalcogen (sulphur, selenium and tellurium) and metal, sub-metal elements readily form stable chemical bonds with oxygen and hydrogen, namely O-H, H_2O, P-O, Ge-O, Ge-H, As-H, CO_2 (*R-O* or *R-H* impurities: *R* is either the chalcogen or *IVB/VB* element) and contribute to a series of undesirable absorption bands in the IR region as summarized in Table 1 [22-26]. For unobscured spectroscopic access, the removal of impurities in raw materials is required. A vacuum drying setup, as shown in Figure 1, for distilling raw materials, was designed and implemented. It consists of three silica ampoules, fused together and attached to a vapour trapping bottle, which is then connected to a vacuum pump. Elemental selenium, tellurium and germanium were placed inside individual silica ampoules. The three ampoules were firstly evacuated to 4×10^{-2} mbar to avoid exposure of elements to ambience. The ampoule containing selenium was heated up to 230°C for 4 hours by removing superficial SeO_2. The ampoule with tellurium was heated in a similar manner but at a much higher temperature at 600°C where the TeO_2 begins to evaporate under reduced pressure. The heating of germanium (Ge) at 450°C was only used to remove free water attached on the surface of raw material.

A very important step in reducing impurities is to clean the silica ampoule with 48% hydrofluoric acid (HF), followed by heating at 1000°C by driving the chemisorbed impurities off from the inner surface. For minimizing the impurity absorption on raw materials, all chemical batching and weighing were carried out inside a glovebox, filled with dried argon gas. After the raw material purification, a 20 g glass batch with composition 20Ge-10Te-70Se (acronymized as a GTS glass) in atomic percent (at%) was prepared for melting. germanium (99.99%), selenium (99.999%) and tellurium (99.99%) were then transferred inside the HF cleaned and vacuum dried silica ampoule. After the batched and weighed material was transferred inside the ampoule, it was evacuated using a high-vacuum (at least 8.0×10^{-6} mbar) before sealing it. High vapour pressures of elemental tellurium and selenium demands extreme precaution during heating inside an evacuated ampoule for preventing pressure build-up leading to explosion. It is for this reason the ampoule must be heated slowly and sufficient time must be allowed for reactions to progress to completion by consuming the high volatile constituents before significant melting begins.

The heating schedule for sealed silica ampoule was controlled at 1°C min^{-1}, with isothermal holds of 2 hours at 250°C and 530°C at which a majority selenium and tellurium, respectively, begin to react. After each hold, the temperature was increased to 950°C at 1°C min^{-1}, at this temperature the furnace was set into a rocking motion for 10 hours for homogenization of liquid formed by dissolving the remaining solid. The temperature was then dropped to 700°C and maintained at this temperature for 2 hours before quenching the ampoule for 20-25 seconds into an ice-cold water bath. The quenched glass was annealed at the glass transition temperature (265°C) for 3 hours to relieve internal stresses. After annealing the glass ampoule was cooled down slowly to the room temperature by turning the furnace power off.

The comparison of impurities in germanium-tellurium-selenium (GTS) glasses before and after purification of raw materials is shown in Fig. 2. It is apparent from this figure that the impurity bonds such as O-H, Ge-O, Se-O and Te-O were significantly reduced after purifying the raw materials. The observed impurities in the purified and unpurified GTS glasses, compared with the literature data [22-26], are summarized in Table 2. The purified glass provides a clear transmission window up to 18 μm (with 2 cm^{-1} absorption coefficient). In an unpurified Ge-Te-Se glass, the large absorption bands between 6.5 and 8.5 μm and 9.0 and 16.0 μm, are the combination of Ge-O, Se-O and Te-O bands which were efficiently reduced. At these wavelengths the apparent loss after raw material purification appears to reach the minimum attenuation of the bulk GTS glass. The apparent increase in absorption at 4.28 and 4.52 μm in glass after purification of a Ge-Te-Se glass are due to the CO/CO_2 and Se-H absorption. The CO/CO_2 may have come from atmosphere during measurements, and the Se-H bonds may have formed during glass melting through the following reaction 1 [27].

$$3Se + 2H_2O \rightarrow 2H_2Se + SeO_2 \tag{1}$$
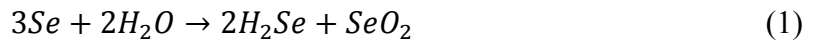
2.2 Preform preparation and fibre drawing

The preform for this multimode chalcogenide fibre was prepared by the extrusion technique. For fibre preform fabrication, the diameter of a core glass needed for extrusion was limited by the

geometry of the ampoule. In our case, the prepared glass rod has 10 mm in diameter and 40 mm in length. Mismatching with the size of the drawing furnace, such a short glass rod cannot be drawn into fibres directly. Practically, a fibre preform at least 70 mm length is required, in order to fit into the isothermal zone of the furnace. Therefore, a cane of 100-120 mm in length and 4-5 mm in diameter was extruded from the short glass rod. The extrusion was carried out in the fibre drawing furnace working between 320°C and 340°C, which was about 55-75°C higher than the glass transformation temperature T_g (in Fig.4). To prevent glass crystallization, the chamber of the furnace was filled with argon gas, maintained at a flow rate of 0.2 liter/min during the extrusion. As illustrated in Fig. 3, a short Ge-Te-Se rod was first placed inside an extrusion mould. By heating the glass inside the extrusion mould inside the furnace and by applying constant pressure from the top through a piston, a thinner glass cane of 4-5 mm in diameter was extruded.

For fibre drawing it is important to control viscosity to prevent crystallization and to maintain flow of material, which yields a uniform shape of the fibre. For GTS glass preform drawing, the thermal properties of the glass was analyzed by using a differential thermal analyzer (DTA), from which the glass transformation temperature T_g (265°C), onset of crystallization temperature T_x (609°C), were recorded, as shown in Fig. 4 (blue curve). Note that at T_x the baseline has shifted down indicating an exothermic process, which is opposite of the endothermic event at T_g. The melting is not shown in this figure. In the viscosity range of 10^5-10^6 Pa.s (Fig.4 black curve), the DTA trace of the Ge-Te-Se glass presents no sharp crystallization peaks, which proves that the glass may be drawn by avoiding devitrification.

From the extruded glass cane, the GTS fibres were drawn at a fixed temperature range between 420°C and 460°C, which corresponds to the 10^5-10^6 Pa.s viscosity. The furnace temperature, feeding and drawing rates were controlled to maintain the fibre drawing as stable as possible. The resulting unclad fibre has a diameter of 110 μm, with ±5 μm variation. Microscopic analysis confirmed that the unclad fibre was clean, smooth and with no obvious crystallization.

3. Fibre characterization

3.1 V-curve

The intrinsic loss defines the theoretical attenuation of a glass which excludes extrinsic loss factors such as crystals and inclusions, transition metals, O-H, water, and other impurities, glass inhomogeneity, air bubble, etc [27-29]. The analysis method for determining the total intrinsic loss has been discussed in reference [30].

   To obtain the V-curve plot of a GTS glass, the UV/visible and infrared spectra were measured using a Perkin-Elmer Lambda 19 UV/visible/NIR spectrometer and a Bruker Vertex 70 FTIR spectrometer. The measured spectra are shown in Fig. 5a. The V-curve was then plotted in Fig. 5b. From this plot, the minimum loss was 0.0003 dB.km^{-1} at 11.5 μm for a 20Ge-10Te-70Se glass. However, this value being a theoretical estimation should only be used as a guide for reducing any extrinsic contributions. When fibre fabrication is carried out, the extrinsic loss factors accumulate and contribute to total loss above the intrinsic loss floor which may be 10^3 to 10^6 times larger, depending upon the processing conditions.

3.2 Fibre loss measurement

The fibre loss measurements were performed with multiple cut-backs by using an FTIR spectrometer (Bruker Vertex 70) with external fibre couplers. Since the spectrometer has a large beam size (around 1 mm), the amount of light coupled into the fibre was low, hence the measured spectra were noisy at longer wavelengths due to mode spreading and low coupling efficiency. However, the multimode GTS fibre used in this investigation had a large core diameter of 110 μm, which enabled coupling light into this fibre with acceptable efficiency. It should be noted that due to unresolved nature of noise in the spectra and low sensitivity of the MCT detector, the measured loss spectra are less reliable at longer wavelengths (>6.8 μm). To minimize the possibility of error and noise in measurements, each spectrum was recorded by multiple scans for 10 times at least, with a 2 cm^{-1} resolution over the whole scanning range. For calculating the fibre loss, multiple cut-back measurements were carried out by recording the transmitted power before and after cutting a piece of fibre (in total 8 cuts was performed, 30 mm of each cut, in-coupling unchanged). The Fresnel reflection induced losses were considered and the measured spectra were corrected

accordingly. Figure 6 shows the loss spectrum, where a transmission window from 1.2 to 6.3 μm with the loss minimum of 1.4 dB/m at 4.2 μm is presented. Moreover, the overall loss was lower than 3 dB/m between 1.5 and 6.3 μm. As expected, the spectrum becomes noisy beyond 6.3 μm due to the detector noise and coupling limitation, which is why the measurements were terminated beyond this wavelength. Another two noise bands appear near 1.2 μm and 2.9 μm, which are due to the UV cut-off edge of the glass and strong fundamental O-H absorption, respectively. In addition, the loss spectrum also presents some impurity absorptions, for instance, the O-H at 2.2 μm, CO/CO_2 at 4.4 μm, Se-H at 4.6 μm and H_2O at 6.3 μm, which are consistent to the absorption spectrum of a bulk glass. Although not all these absorptions were observed in a purified Ge-Te-Se sample (Fig.6, inset figure), it is believed that when the glass was drawn into fibres, the extrinsic loss factors may have contributed to the total loss above the intrinsic loss floor.

4. Theoretical verification of FEWS sensing using a unclad Ge-Te-Se fibre

4.1 Analysis of optical modes in the Ge-Te-Se fibre

To use a multimode Ge-Te-Se fibre for FEWS sensing, an important factor is to consider the optical modes in the fibre. Previous studies using either unclad, or removed cladding, multimode chalcogenide fibres for FEWS sensing, with core diameters ranging from 100 to 400 μm, have been reported extensively [1, 3, 8, 9, 31-34]. It is also known that by tapering down a fibre with sub-wavelength features can also improve FEWS sensing since large proportion of light cannot be confined in to the fibre core which propagates along the fibre surface [18,19]. However, unlike silica, which can be easily tapered down to nano-scale, most chalcogenide glass fibres are difficult for post-processing due to thermal instability and poor mechanical strength [19, 27-29]. There are two main advantages for using a multimode Ge-Te-Se fibre in this investigation. Firstly, the fibre has a core diameter of 110 μm which supports a multitude of optical modes. Compared to fundamental mode, the higher order modes (HOMs) can penetrate further into cladding medium, and therefore enhance the measurement sensitivity. This can be understood with the following equations. In an optical fibre, an evanescent field decays into the cladding medium by equation 2 [35]

$$E_{cladding}(y) = E_{cladding}(0)e^{-\alpha_{cladding}y} \tag{2}$$

where $E_{cladding}(y)$ is the field in the cladding layer at a position y measured from the boundary and $E_{cladding}(0)$ is the boundary field. $\alpha_{cladding}$ is the decay coefficient in the cladding medium and can be calculated through equation 3 [3, 35]

$$\alpha_{cladding} = \frac{2\pi}{\lambda}\sqrt{n_{eff}^2 - n_{cladding}^2} \tag{3}$$

where n_{eff} is the effective refractive indices of optical modes and $n_{cladding}$ is the refractive index of the cladding medium.

The mode field width (MFW) of evanescent wave is defined as the penetration depth when the field $E_{cladding}(y)$ decayed to e^{-1} of the $E_{cladding}(0)$. According to equations 2 and 3, y is then defined as the penetration depth d_p at this position by

$$y = {1}/{\alpha_{cladding}} = {\lambda}\left/{2\pi\sqrt{n_{eff}^2 - n_{cladding}^2}}\right. = d_p \tag{4}$$

It is known that in a multimode fibre, the effective mode indices of HOMs are smaller than that of the fundamental mode. Therefore, the penetration depths d_p of HOMs are always larger, compared to that of the fundamental mode.

Another benefit of using a multimode fibre is the improved coupling efficiency. As mentioned before, we used an FTIR spectrometer with a mercury-cadmium-telluride (MCT) detector as a light source. The beam diameter of the light source was about 1 mm. The fibre in-coupling or out-coupling was achieved through free-space mirror optics, which is non-trivial if the fibre diameter is reduced much lower than 100 μm.

Although in previous investigations the multimode chalcogenide fibres were extensively discussed for FEWS sensing, until now, the influence arising from HOMs was never discussed. The FEWS sensing is based on spectrum analysis. We can assume the variations in spectra rely on changes in sensing species, and are independent of optical modes if a coupled mode does not convert to other higher/lower order modes because of fibre bending or external disturbance during measurements, which may lead to a drop/increase of output power. To verify this assumption, a theoretical study was performed using the finite element method. Figure 7 shows the results of the

simulation. The calculation was based on a model with the same parameters as the GTS fibre used in the experiment. In the model, a perfect matched layer (PML) was added to avoid reflections at the boundary and the multimode fibre was surrounded by water. Figure 7a shows a quarter of the profile of the fundamental mode LP_{01} (the full mode profile is shown in Fig. 7c) where the penetration of the evanescent field (in log scale) into the surrounding medium may be observed (the fibre core region was marked with a black solid line near the right-bottom corner). There is not a significant difference in the penetration depth of the evanescent field when comparing the profile of the LP_{01} mode with that of a HOM LP_{21} in Fig. 7b. As expected, the computation confirms that the GTS fibre supports many optical modes. Figure 7d-7j give the patterns of selected lower order HOMs, namely the LP_{21}, LP_{31}, LP_{81}, LP_{02}, $LP_{03,}$ LP_{12} and LP_{13}. It is true that many other HOMs are supported in this fibre but considering that their confinement losses are relatively high, the analyses of these lower order HOMs in Fig.7 should be sufficient to understand the influence of HOMs in a FEWS fibre sensor.

4.2 Penetration depths under different circumstances

Figures 7a and 7b present the field distribution of the LP_{01} and LP_{21} modes. From these two figures, the difference in the penetration depths of the two modes is indistinguishable into the cladding medium. For improving this analysis, a one-dimensional (1D) mode profile was plotted to show the intensity variations along a line through the fibre center on its 2D transverse plane in Fig. 7, which is shown in Fig. 8a. The two red dash-lines at 110 μm define the boundaries of the GTS fibre. It is clear that the light is well-confined within the fibre due to high index of the GTS glass. Different optical modes, however, exhibit different modal distribution, which is apparent from the 1D plot (Fig. 8a). It is also found that near the boundary of the fibre, the intensity of light decays exponentially into the cladding medium, no matter which modes are considered. Figure 8b enlarges the high-lighted red rectangle region in Fig. 8a, showing the intensity decay at the fibre boundary (grey area presents the GTS glass). As expected, the fundamental mode LP_{01} has the lowest mode intensity at the boundary than that of the HOMs. Above the boundary of the fibre, the HOMs, e.g. LP_{81}, can have more light penetrated into the cladding medium. A closer

examination of the intensity variation near the boundary of the fibre is shown in Fig. 8c, from which the calculated intensity of the LP_{81} mode is clearly seen to be at least an order of magnitude (>10 times) higher than that of the LP_{01} mode, at the fibre boundary. Summarized from Fig. 8c, a 1D plot of mode intensities versus optical modes is compared in Fig. 8d. In the ascending order of intensities, the modal intensities are as follows: $LP_{01} < LP_{21} < LP_{12} < LP_{02} < LP_{13} < LP_{03} < LP_{81}$, consistent with the values of effective mode indices given by the finite-element calculations. Table 3 shows the calculated effective refractive indices of different modes.

It was expected that by coating the fibre with inorganic materials such as diamond, Ta_2O_5 or TiO_2 can either avoid the direct contact of the fibre with chemical species, or improve the sensitivity. To verify this assumption, more calculations were performed. A thin layer (50-500 nm) of diamond, Ta_2O_5 or TiO_2 on the fibre surface was included in the model. The calculated results are compared in Fig. 9. Obviously, after coating the evanescent field is significantly interrupted, as can be observed from the computed values in Fig.9b-9d. Only small amount of light can penetrate through these coating layers, as compare with that of an uncoated fibre (Fig. 9a). The computed results are consistent when a step-index core-clad fibre is used for FEWS sensing. In this case the cladding layer needs to be removed by etching/polishing to allow as much light as possible to reach the boundary. Figure 9e plots the mode profiles under different circumstances (the 0 point represent the fibre center with a core diameter of 110 μm). The data on y-axis was firstly normalized and then plotted on a log scale. It can be seen that in the fibre without any coating, the propagating light penetrates through the fibre surface with much higher intensity, as compared with other cases. Therefore, in order to maximize the measurement sensitivity, we chose not to apply any coating on the Ge-Te-Se fibre for the sensing experiments.

5. Fibre evanescent wave spectroscopic sensor

5.1 Experimental setup

With the understanding of the intensity distribution of optical modes as well as penetration depths in the unclad GTS fiber, we designed and fabricated a FEWS sensor as shown in Fig. 10. A short piece of Ge-Te-Se fibre (40 cm long) was coupled with a Bruker Vertex 70 FTIR spectrometer and an MCT infrared detector using free-space optics. The two ends of the fibre were mounted on

3-axis translation stages. The in-coupling light beam from the spectrometer, after propagating through the fibre, was then coupled out into the MCT detector. The in/out-coupling was realized with two parabolic mirrors based on light reflection instead of transmission to avoid material absorption at long wavelengths. In this setup, the Ge-Se-Te fibre worked as the light delivery medium, as well as the sensing probe. In the middle of the fibre, a small container with two side holes was designed to let the fibre sit in without bending. About 3 cm fibre was kept fully immersed into the analyte medium. As discussed before, the effective spectral range for sensing was limited in the 1 to 6.8 μm.

Several chemical species which commonly occur in food and pharmaceutical manufacturing were used for sensing experiments. Diluted acetone (CH_3COCH_3 99%), acetic acid (CH_3CO_2H, 99%), ethanol (CH_3CH_2OH, 95%), methanol (CH_3OH, 99%) solutions with various concentrations were tested. Methanol is a toxic substance and must be controlled during the synthesis of ethanol which is why we have characterized the concentrations. Tocopherol (vitamin E capsule, Holland & Barrett), ascorbic acid (vitamin C tablet, Holland & Barrett) and freshly squeezed lemon and orange juice were also verified using this sensor in a range of concentrations, shown below. It was interesting to find that some species such as tocopherol and ascorbic acid can easily attach to the surface of the fibre and hence contributed to strong absorption of the evanescent field.

The main absorption bands of the above chemical species distributed in three spectral regions are 2.9-3.8, 5-6 and 6-8 μm [36]. Specifically, the absorptions between 2.9 and 3.8 μm are attributed to the C-H stretching and the fundamental O-H stretching vibrations [1, 36, 37]. The bands in 5-6 μm are assigned to the overtones and combination bands of C=O stretching vibrations [1, 3, 37], and the absorptions in the 6-8 μm region are due to the ring C=C and C-H vibrations [3, 37].

The measurements were implemented by first recording the background spectrum as $P_{background}$, without sensing species, and then by measuring the transmission spectrum as P_{sample} with chemical solutions in the container. The absorption spectrum was then calculated through equation 5.

$$\alpha_{transmission} = {P_{sample}}\Big/{P_{background}} \qquad (5)$$

The Sigma library of FTIR spectra [36] provides a complete database of infrared transmission/absorption spectra of most chemicals. The data can be used as references for the analysis. In order to locate the positions of absorption peaks accurately, the measured spectra were deconvoluted into symmetrical Gaussian peaks, as depicted in Figures 11 to 14.

5.2 Results and discussion

a. Ethanol and methanol

Ethanol solutions with concentration from 10 to 100% were used for the experiments. The chemical formula (Fig. 11a, inset figures) indicates that ethanol should have C-H and O-H stretching vibrations between 2.9 and 3.8 μm. With the FEWS sensor, a broad absorption band from 3.3 to 3.6 μm, including two distinct peaks at 3.362 μm and 3.472 μm, and two weaker peaks at 3.401 and 3.535 μm, are reported. From the Sigma FT-IR database, the IR characteristic peaks of ethanol are at 3.362, 3.482, 4.039 and 6.911 μm. The two intense peaks at 3.362 and 3.471 are consistent with the database. However, the other two observed peaks at 3.401 and 3.535 μm cannot be used as characteristic fingerprints as they are relatively weaker and cannot be distinguished from the main absorption bands. The fourth peak at 6.911 μm from the Sigma database is beyond the detection range of this sensor, therefore, was not observed. When the solution was diluted to 10%, the spectra still present a relatively high absorption at 3.362 and 3.471 μm, which suggests this type of FEWS sensor might be useful for the analysis at lower concentrations.

In food industry it is important to speciate the contamination of methanol from ethanol, because of its irreversible toxicity leading to blindness in human beings, when consumed. The absorption bands of methanol should be comparable with that of ethanol, as both of them have C-H and O-H stretching vibrations. However, the bonding force and bonding distance of a chemical bond can be very different in molecular species, even though the constituent elements may be identical. Figure 11b shows the absorption spectra of methanol with concentrations ranging from 5% to 100%. The peak positions are located at 3.115, 3.398 and 3.536 μm. From the Sigma database, the IR

characteristic peaks of 99% methanol should be at 2.992, 3.398, 3.546 and 6.897 µm. In the experiments, we were not able to see the last peak as it exceeds the sensing range of the sensor. However, all the other three peaks are consistent with the database.

Further analyses of the measured data are shown in Fig. 12, where the absorption coefficients of ethanol and methanol with varied concentrations are plotted at different absorption wavelengths. The absorption coefficient in cm^{-1} corresponds to the attenuation in dB/m by a product factor of 10^3, which indicates the detection limit can be further improved for ppm or even sub-ppm measurements if a suitable detector is used.

b. Acetone

Acetone has several strong absorption bands in the mid-IR regions at 3-3.4, 4.2-5.0, 5.5-6.2 and 6.3-7.2 µm, as shown in Fig. 13. Absorption spectra of 5 to 70 vol% acetone solutions were measured using this FEWS sensor. The chemical formula (Fig. 13, inset figures) suggests that both C=O and C-H stretching vibrations may exist, which contribute to absorption at 3.177, 4.681, 5.868 and 6.091 µm. The positions of the first three peaks are consistent with the ones in the Sigma FTIR data at 2.947, 4.432 and 5.866 µm [36]. The absorption peak at 5.86 µm was also reported by Heo [3]. The slight shift in peak positions may be due to the presence of water in all solutions. The water weakens acetone and creates more H$^+$ ions which can shift the absorption at specific wavelengths. From Fig. 13, it is found that even after the concentration was reduced to 5 vol%, strong absorption still exists in the spectra, and the sensor continues to detect lower concentrations.

c. Acetic acid

The absorption spectra of acetic acid solutions (5 - 90 vol.%) were measured as shown in Fig. 14. There are several absorption peaks at 3.221, 4.765, 5.837 and 6.066 µm. These absorption peaks are the results of the C-H, O-H and C=O stretching vibrations which may be compared with the Sigma absorption database at 3.287, 3.800, 5.833 and 7.076 µm. The apparent difference in peak position arises due to the presence of water, which creates more H$^+$ ions in the solutions. It must be pointed that when the concentrations of acetic acid was reduced to 5 vol%, most absorption

disappeared and we were unable to identify the peaks from the background noise. However, by performing multiple scans or increasing the sensing fibre length, this problem may be solved.

d. Vitamin C, E and squeezed fresh lemon/orange juice

It is well known that the main constituents of vitamin E and vitamin C are tocopherol and ascorbic acid, respectively, which we also targeted for the characterization using the Ge-Te-Se FEWS sensor. Our target concentration range in solutions for the two vitamins was in the ppm range. The analyte solutions were prepared from the commercial pills or capsules, bought from Holland and Barrett departmental store. A vitamin E capsule contains 136 mg vitamin E dissolved in vegetable oil. When diluting it with water, the oil remains immiscible. Due to this reason, the solution was stirred thoroughly by using a hot plate and a magnetic stirrer to make the oil droplets dispersed homogeneously. One vitamin E in 200 g water yields a tocopherol concentration of 680 ppm. A multi-vitamin tablet contains 20 mg vitamin C, which was then dissolved in 40 g water, which produces 500 ppm concentration of ascorbic acid. The prepared vitamin E and C solutions were then used for sensing experiments. The measured spectra are shown in Fig. 15a. Besides C-H, C=O vibrations, both species have ring C=C bonds. Unfortunately, as the corresponding absorption sits between 6 and 8 μm, it was not possible to detect these bands using this sensor due to the limitation on fibre coupling in the FTIR. For vitamin E, the absorption peaks are located at 3.418, 3.473 and 5.731 μm, which are consistent with the Sigma database where the characteristic absorptions were reported at 3.417, 3.474 and 5.731 μm.

In conclusion, the designed FEWS sensor yielded reliable results in the low concentrations of 680 ppm. For vitamin C, the observed absorption bands are at 3.183, 4.752, 5.902 and 6.031 μm. Although there are small differences between the measurements and Sigma database, the positions of main peaks are consistent with each other. It must be pointed out that the absorption intensities for both the vitamin E and C solutions are strong in the ppm range, which indicate that the concentration may be further reduced and determined accurately using the absorption peaks. The possible reasons for high sensitivity with these two species can be explained as below. As already mentioned, some chemicals are easy to attach to the surface of the fibre due to suitable particle

sizes and surface activity, which increases the absorption of evanescent field and hence contribute to high sensitivity [1, 3]. We believe that the sensitivity can be further improved for sub-ppm measurements by using FEWS technique, discussed above by enhancing the possibility of attracting molecules to fibre surface, increasing the number of scans, and the length of the sensing zone, and above all fibre coupling and detector sensitivity.

It is well known that both lemon and orange contain abundant amount of vitamin C, on average 40 mg and 35 mg of vitamin C, respectively in each fruit. For sensing experiments, each fruit juice was squeezed and the juice was transferred into the analyte dish with FEWS. The absorption spectra of juice samples are shown in Fig. 15b. The results are similar to that of the vitamin C solution.

Table 4 concludes the positions of characteristic absorption of different chemical species studied by the designed FEWS.

Further improvement in sensor design may be feasible using a hollow-core ARROW fibre design for future fibre sensing applications, especially when considering the GTS glass type extended IR medium. Such a novel fibre may capable of performing simultaneous gas/liquid suspension analysis for industry.

6. Conclusion

A simple and robust fibre evanescent wave spectroscopic sensor using a multimode chalcogenide fibre was designed and constructed for chemical sensing. A comprehensive review of methodologies adopted for material development and fiber drawing was presented in the following steps: purification of raw chemicals for high spectral purity, glass melting, quenching and annealing, fabrication of fiber preform and finally, fibre drawing. The fabricated unclad fibre of 110 μm has a minimum loss of 1.4 dB/m at 4.24 μm, and less than 3 dB/m between 1.5 and 6.3 μm. The finite-element (FE) calculations was applied for characterizing the modal intensity distribution and their respective penetration depth into the analyte medium. Based on the simulation, a FEWS sensor with 3 cm sensing zone was constructed. Chemical species from food and pharmaceutical products were studied by means of spectroscopic analysis with this sensor.

The sensitivity of the sensor has been verified in the ppm concentration range for vitamins. Methods for improving the sensor sensitivity by increasing the path length and detector sensitivity are proposed.

Reference:

[1] J. S. Sanghera, F. H. Hung, L. E. Busse, P. C. Pureza and I. D. Aggarwal, "Infrared evanescent absorption spectroscopy of toxic chemicals using chalcogenide glass fibers", J. Am. Ceram. Soc., **78**, 2198-2202 (1995).

[2] F Yu, W. J. Wadsworth, J. C. Knight, "Low loss silica hollow core fibers for 3-4 μm spectral region," Opt. Express, **20**, 11153 (2012).

[3] J. Heo, M. Rodrigues, S. J. Saggese and G. H. Sigel, "Remote fiber-optic chemical sensing using evanescent-wave interactions in chalcogenide glass fibers", Appl. Opt., **30**, 3944-3951 (1991).

[4] M. Saito, M. Takizawa, K. Ikegawa and H. Takami, "Optical remote sensing system for hydrocarbon gases using infrared fibers", J. Appl. Phys., **63**, 269 (1988).

[5] S.J. Saggese, M.R. Shahriari and G.H. Sigel, Jr., "Fluoride fibers for remote chemical sensing" Proc. SPIE **929**, 106 (1988)

[6] S. Simhony, E. M. Kosower and A. katzir, "Novel attenuated total internal reflectance spectroscopic cell using infrared fibers for aqueous solutions", Appl. Phys. Lett. **49**, 253-254 (1986)

[7] R.J. Burger, P.J. Melling, W.A. Moser and J.R. Berard, "Remote spectroscopy using mid-IR fiber-coupled laboratory apparatus" Proc. SPIE **1591**, 256 (1991)

[8] J.S. Sanghera, F.H. Kung, P.C. Pureza, V.Q. Nguyen, R.E. Miklos and I.D. Aggarwal, "Infrared evanescent-absorption spectroscopy with chalcogenide glass fibers" App. Opt., **33**, 6315 (1994)

[9] D. L. Coq, K. Michel, J. Keirsse, C. Boussard-Pledel, G. Fonteneau, B. Bureau, J. L. Quere, O. Sire and J. Lucas, "Infrared glass fibers for in-situ sensing, chemical and biochemical reactions", C.R.Chimie, **5**, 907-913 (2002)

[10] R. Fairman and B. Ushkov, *Semiconducting chalcogenide glass III: applications of chalcogenide glasses*, London: Elsevier Science Publishing Co Inc (2004).

[11] H. J. Arditty, J. P. Dakin and R. T. Kersten, eds., Optical fiber sensors, Springer-Verlag, Berlin (1989).

[12] M. Saito and K. Kikuchi, "Infrared optical fiber sensors," Opt. Rev., **4**, 527-538 (1997)

[13] F.S. Ligler and Chris A.Rove Taitt, Optical biosensors: present and future, Amsterdam, Elsevier, Oxford (2002)

[14] S. Simhony, E. M. Kosower and A. katzir, "Novel attenuated total internal reflectance spectroscopic cell using infrared fibers for aqueous solutions" App. Phys. Lett. **49**, 253-254 (1986)

[15] A. Messica, A. Greenstein and A. Katzir, "Theory of fiber-optic, evanescent-wave spectroscopy and sensors", Appl. Opt., **35**, 2274-2284 (1996)

[16] P. S. Kumar, C. P.G. Vallabhan, V. P. N.Nampoori, V. N. S. Pillai, P. Radhakrishnan, "A fibre optic evanescent wave sensor used for the detection of trace nitrites in water," J. Opt. A: Pure Appl. Opt., **4**, 247 (2002).

[17] L. C. Shriver-lake, G. P. Anderson, J. P. Golden and F. S. Ligler, "The effect of tapering the optical fiber on evanescent wave measurements," Analy. Lett., **25**, 1183-1199 (1992).

[18] L.M. Tong, R. R. Gattass, J. B. Ashcom, S. L. He, J. Y. Lou, M. Y. Shen, I. Maxwell, E. Mazur, "Subwavelength-diameter silica wires for low –loss optical wave guiding," Nature, **426**, 816-819 (2003).

[19] G. Brambilla, "Optical fibre nanowires and microwires: a review," J. Opt., **12**, 1-19 (2010).

[20] Y. H. Tai, P. K. Wei, "Sensitive liquid refractive index sensors using tapered optical fiber tips, " Opt. Lett., **35**, 944-946 (2010).

[21] P. Wang, G. Brambilla, M. Ding, Y. Semenova, Q. Wu, G. Farrell, "High-sensitivity, evanescent field refractometric sensor based on a tapered, multimode fiber interference," Opt. Lett., **36**, 2233-2235 (2011).

[22] T. Katsuyama, K. Ishida, S. Satoh and H. Matsumura, "Low loss Ge-Se chalcogenide glass optical fiber," Appl. Phys. Lett., **45**, 925-927 (1984).

[23] M. F. Churbanov, "High-purity chalcogenide glasses as matrials for fiber optics," J. Non-Cryst. Solids, **184**, 25-29 (1995).

[24] V. S. Shiryaev, J. L. Adam, X. H. Zhang, C. Boussard-Pledel, J. Lucas and M. F. Churbanov, "Infrared fibers based on Te-As-Se glass system with low optical losses," J. Non-Cryst. Solids, **336**, 113-119 (2004).

[25] V. S. Shiryaev, C. Boussard-Pledel, P. houizot, T. Jouan, J. L. Adam, andJ. Lucas, "Single-mode infrared fibers based on Te-As-Se glass system," Mater. Sci. Eng. B, **127**, 138-143 (2006).

[26] A. R. Hilton and C. E. Jones, "Non-oxide IVA-VA-VIA chalcogenide glasses. Part 2. Infra-red absorption by oxide impurities," Phys. Chem. Glasses, **7**, 112-116 (1966).

[27] V.F. Kokorina, *Glasses for Infrared Optics*, Boca Raton: CRC press (1996).

[28] J.A. Harrington, *Infrared fibers and their applications*, Bellingham, Washington: SPIE-The International Society for Optical Engineering
(2004).

[29] J.S. Sanghera and I.D. Aggarwal, *Infrared fiber optics*, Boca Raton:CRC Press Inc (1998)

[30] X. Jiang, J. Lousteau, B. Richards and A. Jha, "Investigation on germanium oxide-based glasses for infrared optical fibre development", Optical Materials, **31**(11), 1701-1706 (2009).

[31] S. Hocde, C. Boussard-Pledel, G. Fonteneau, J. Lucas, "Chalcogens based glasses for IR fiber chemical sensors," Solid. State. Sci. **3**, 279-284 (2001).

[32] D.Le Coq, C. Boussard-Pledel, G. Fonteneau, T. Pain, B. Bureau, J.L. Adam, "Chalcogenide double index fibers: fabrication, design and application as a chemical sensor", Mater. Res. Bull., **38**, 1745-1754 (2003).

[33] K. Michel, B. Bureau, C. Boussard-Pledel, T. Jouan, J. L. Adam, K. Staubmann, T. Baumann, "Monitoring of pollutant in waste water by infrared spectroscopy using chalcogenide glass optical fibers," Sensors. Actuators B: Chemical, **101**, 252-259 (2004).

[34] F. Charpentier, B. Bureau, J. Troles, C. Boussard-Pledel, K. M. Pierres, F. Smektala, J. L. Adam, "Infrared monitoring of underground CO_2 storage using chalcogenide glass fibers," Opt. Mater., **31**, 496-500 (2009).

[35] S. O. Kasap, *Optoelectronics and Photonics: Principles and Practices*, Upper Saddle River, New Jersey: Prentice-Hall (2001).

[36] R.J. Keller, *The sigma library of FT-IR spectra*, eds 1, Sigma Chemical Company, INC. St. Louis, Missouri (1986).

[37] J. Keirsse, C. Boussard-Pledel, O. Loreal, O. Sire, B. Bureau, P. Leroyer, B. Turlin and J. Lucas, "IR optical fiber sensor for biomedical applications," Vib. Spectrosc., **32**, 23-32 (2003).

[38] P. Lucas, D. L. Coq, C. Juncker, J. Collier, D. E. Boesewetter, C. Boussard-Pledel, B. Bureau and M. R. Riley, "Evaluation of toxic agent effects on lung cells by fiber evanescent wave spectroscopy (FEWS)," Appl. Spectrosc., **59,** 1-9 (2005).
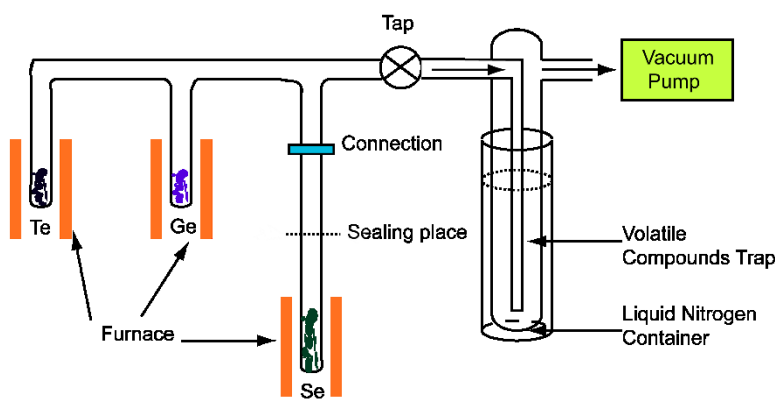
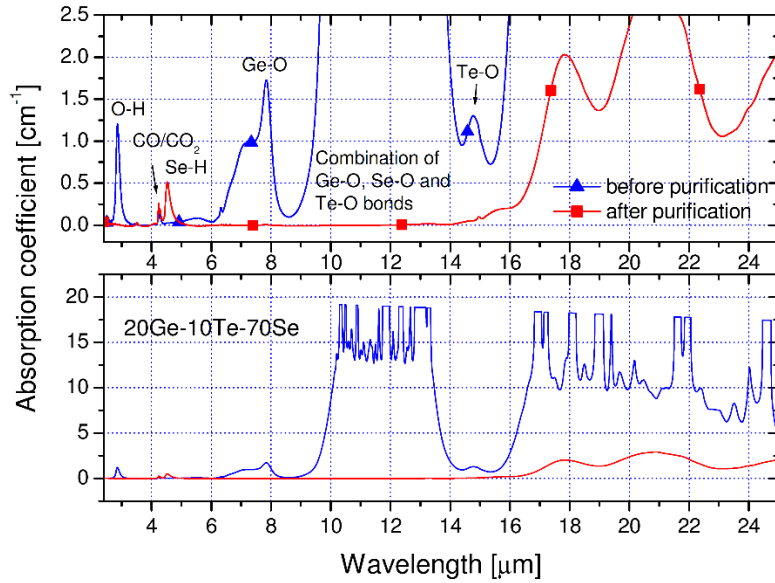**Fig. 1 Experimental setup of a vacuum drying system for the purification of raw chemicals.**

Fig. 2 Absorption spectra of the 20Ge-10Te-70Se glasses before (blue) and after (red) purification of raw materials. The upper figure shows the enlarged spectra with impurity bonds marked on each absorption peak/band; the lower figure presents the full spectra between 2.5 and 25 μm.
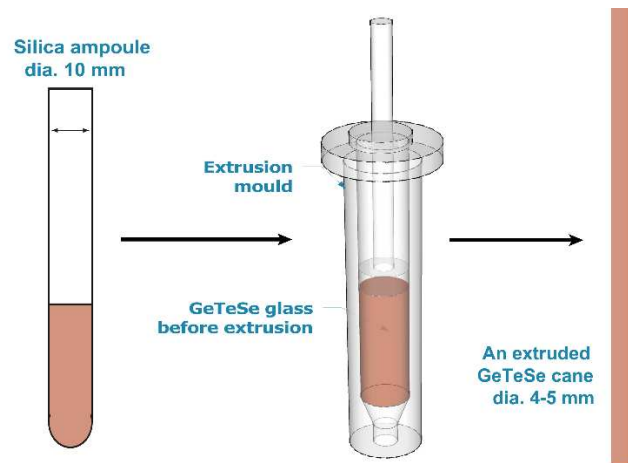

Fig. 3 Schematic illustration of the preparation of a chalcogenide fibre preform using the extrusion technique. The prepared Ge-Te-Se glass rod (~40 mm in length) can be extruded into a thin rod of ~120 mm long, which is suitable for fibre drawing. During extrusion, inert gas protection is purged into the extrusion mould.
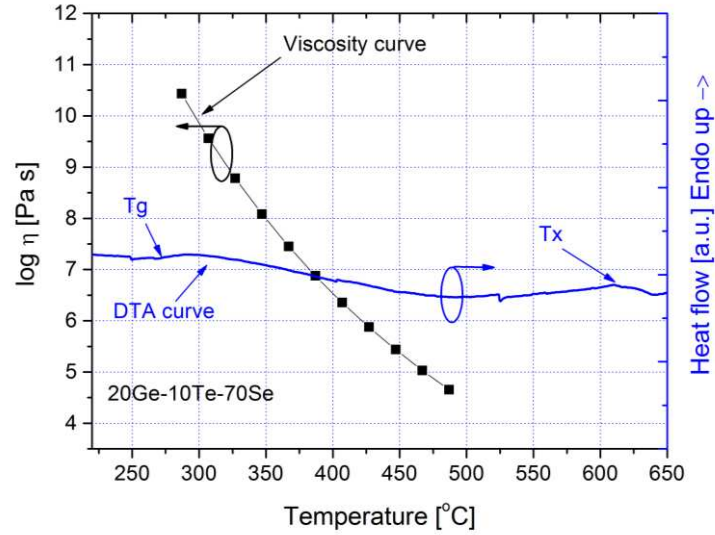
Fig. 4 The viscosity in Pa.s (left Y-axis) and DTA scan (right) (heat flow measured as ΔT) curves of a 20Ge-10Te-70Se glass
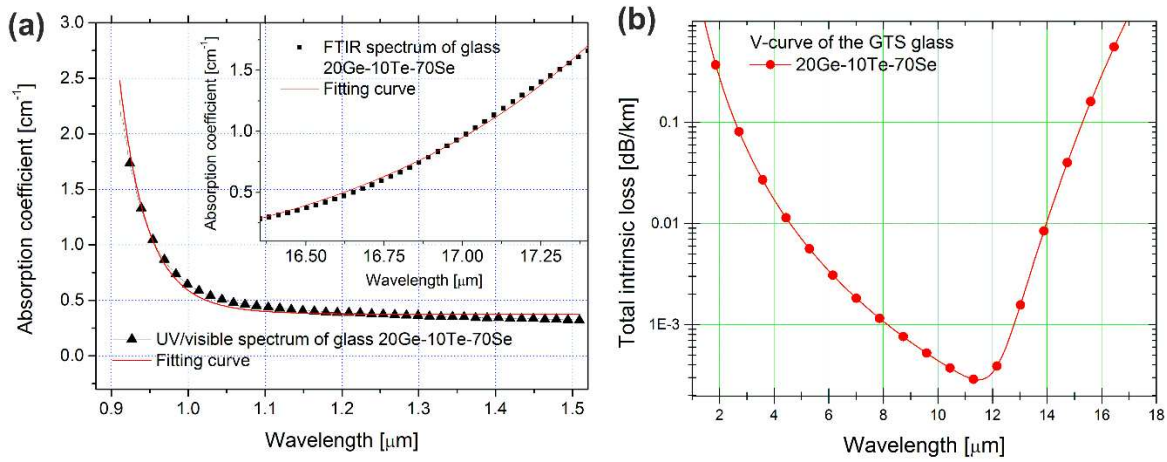
Fig. 5 (a) UV/visible and FTIR absorption spectra of 20Ge-10Te-70Se glass. Red solid lines are fits for the spectra; (b) A V-curve plotted with the fitting constants from the UV/visible and infrared spectra. The V-curve is the theoretical estimation of the intrinsic loss for the glass.
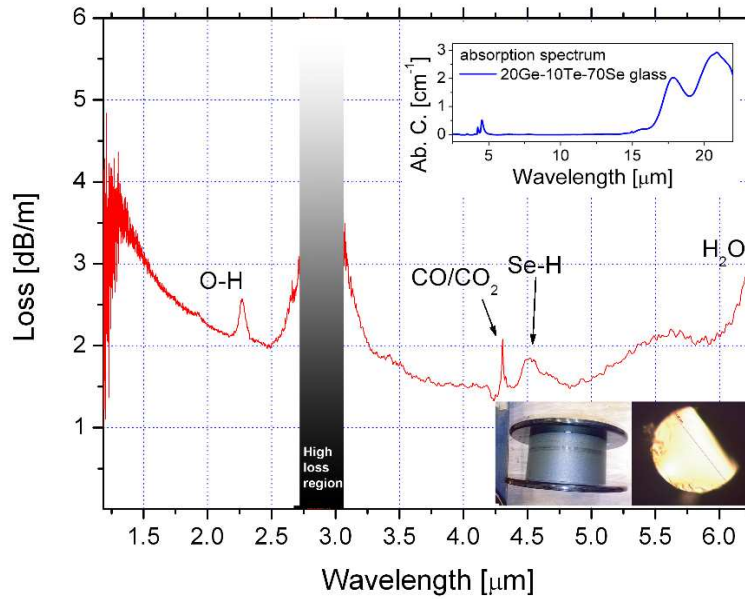
Fig. 6 Loss sepectrum of the 20Ge-10Te-70Se chalcogenide glass multi-mode fibre, measured by a FTIR spctrometer using the cut-back method. The noise band close to 1.2 µm is due to the UV cut-off of the glass, whereas the other high loss region at around 2.9 µm is due to the sensing limitation of the MCT detector. Absorptions due to other impurities are marked on the spectrum. The inset figure (upper) show absorption spectrum of the bulk glass, and the lower ones show the fibre on a spool and a microscopic graph of the cross section.
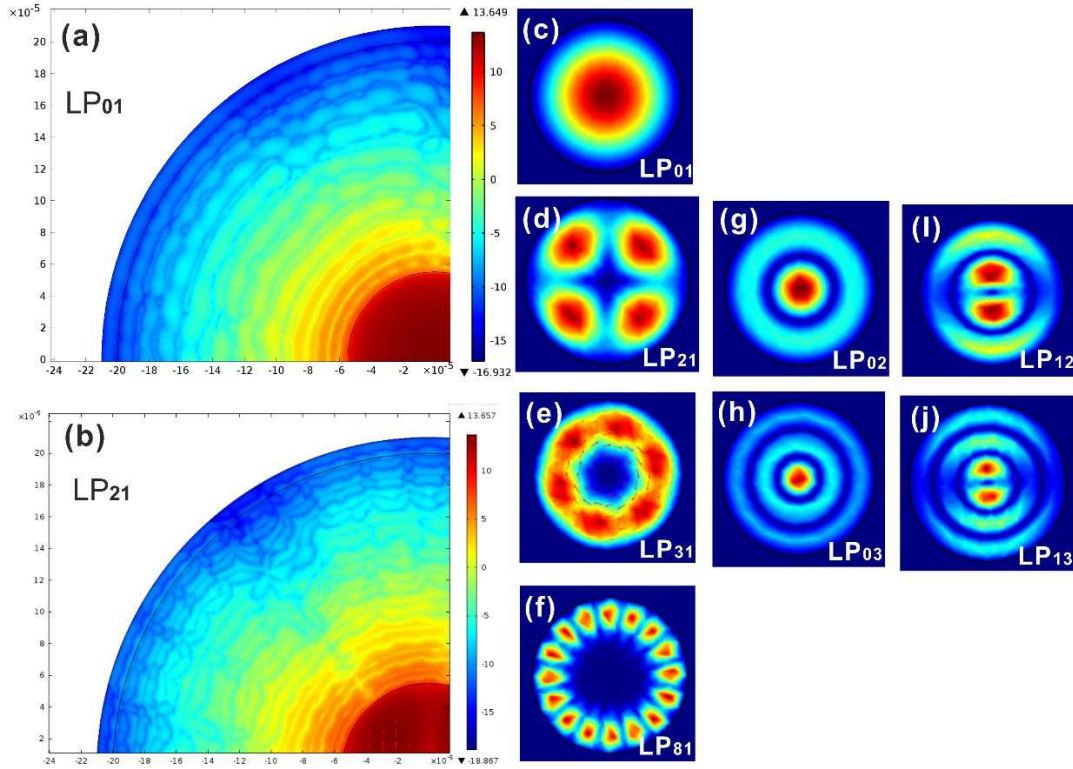
Fig. 7 Calculated modes supported by the multi-mode 20Ge-10Te-70Se fibre at 3.5 µm. (a) and (b) The penetration of the evanescent field of the LP$_{01}$ and LP$_{21}$ modes into the surrounding medium may be clearly seen (the fibre core region was marked with a black solid line near the right-bottom corner). (c)-(j) present the calcualted optical modes including the fundamental mode LP$_{01}$ and some HOMs in the 20Ge-70Se-10Te fibre. The calculation was performed by using the finite element method. Perfect matched layer was added and the fibre was assumed to be surrounded by water.
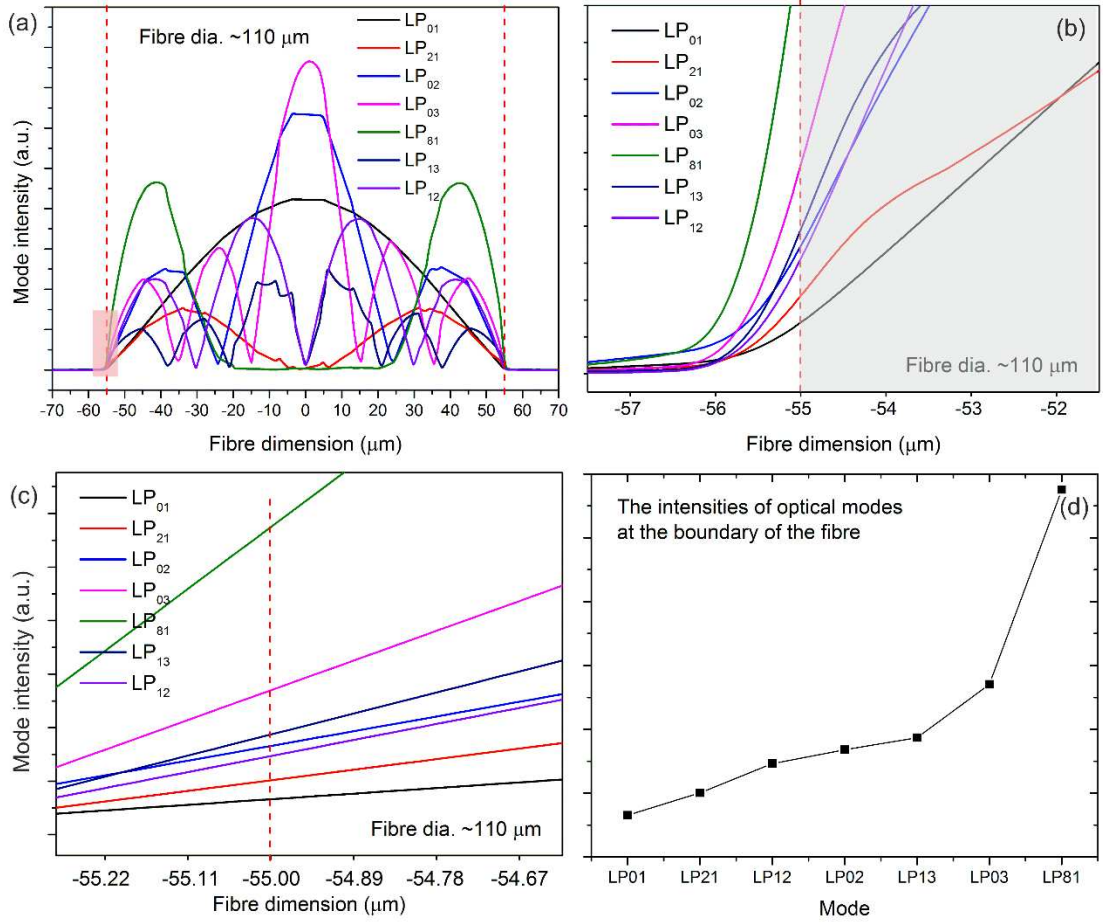
Fig.8 (a) 2D plots of field intensities of different modes, and (b) enlargred region in Fig. 8a (red square), near the edge of the fibre. The grey area shows the fibre and the vertical dash line is the edge. (c) and (d) Comparasion of intensity variation at the boundary of the fibre from different modes.
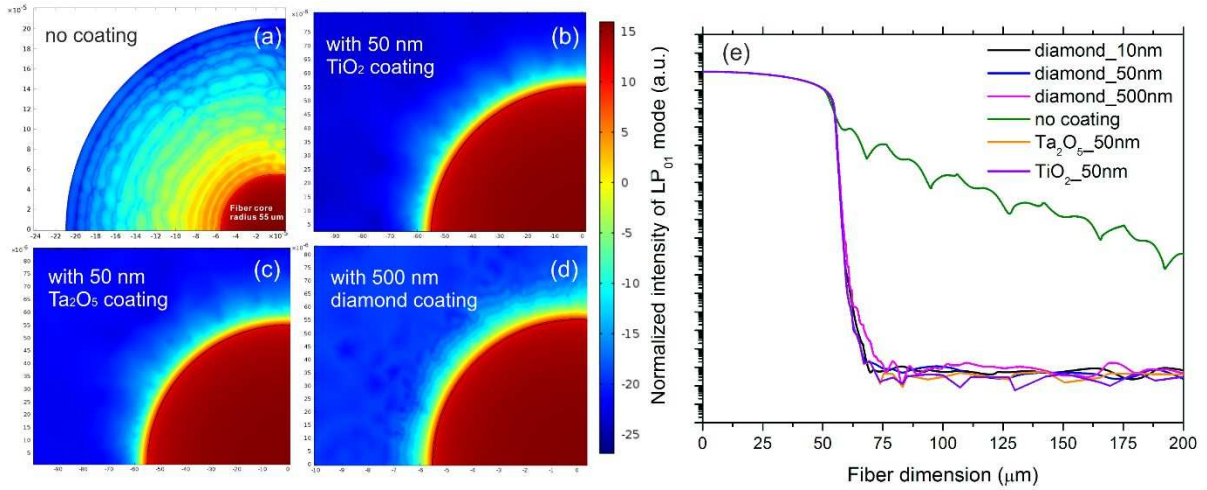
Fig. 9 Calculated LP$_{01}$ mode profiles in 20Ge-10Te-70Se fibres (a) without coating , (b) with 50 nm TiO$_2$ coating, (c) with 50 nm Ta$_2$O$_5$ coating and (d) with 500 nm diamond coating. Figure (e) shows the 1D plot of field distribution under different circumstances.
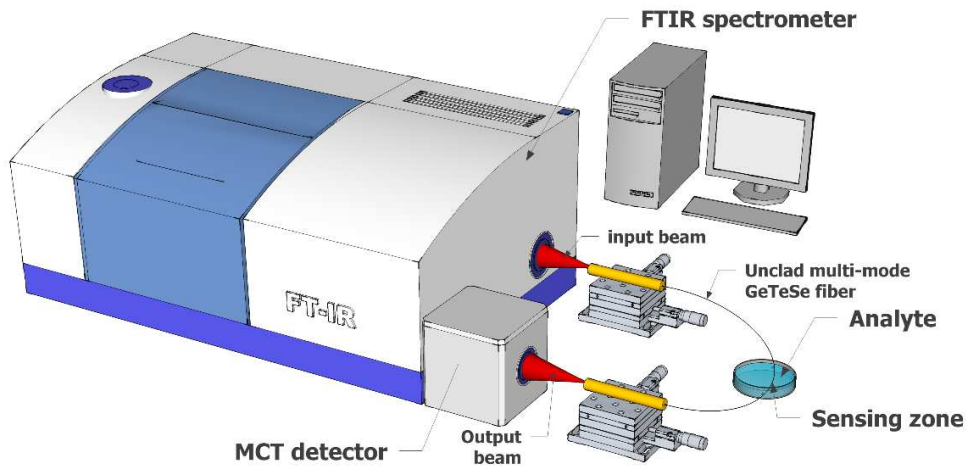

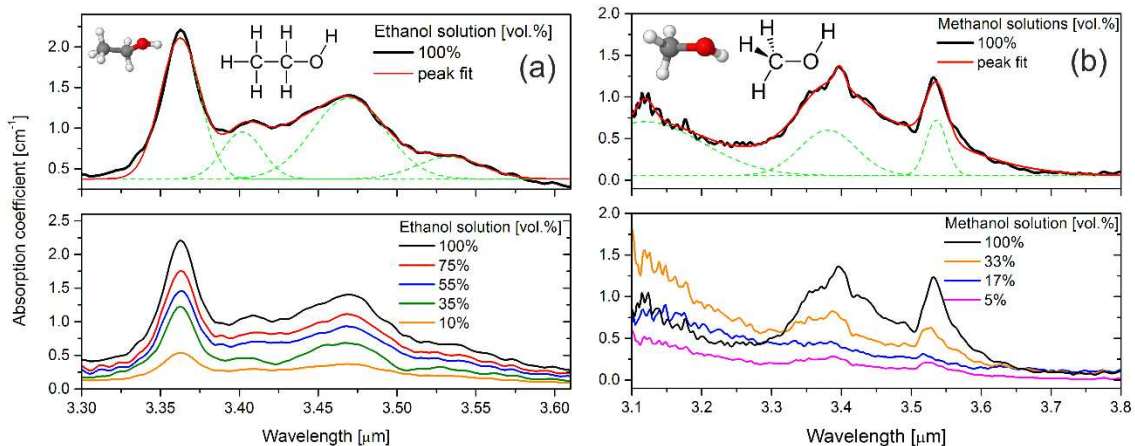**Fig. 10** Experimental setup of a fibre evanescent wave spectroscopic sensor.

Fig. 11 Absorption spectra of ethanol (a) and methanol (b) solutions with the concentration ranging from 10 to 100 vol.%, and 5 to 100 vol.%, respectively. The upper figures show the peak fit for the spectra (the inset figures show of the structural formula and ball-and-stick models). The green dash lines present the fitted peaks, Guassian shape assumed.
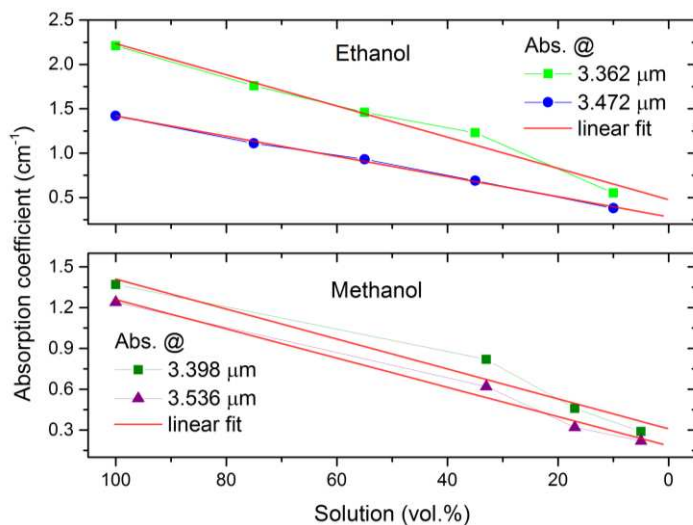

Fig. 12 Measured absorption coefficients of ethanol and methanol solutions at various absorption peaks. The red solid lines are fits for the measured data.
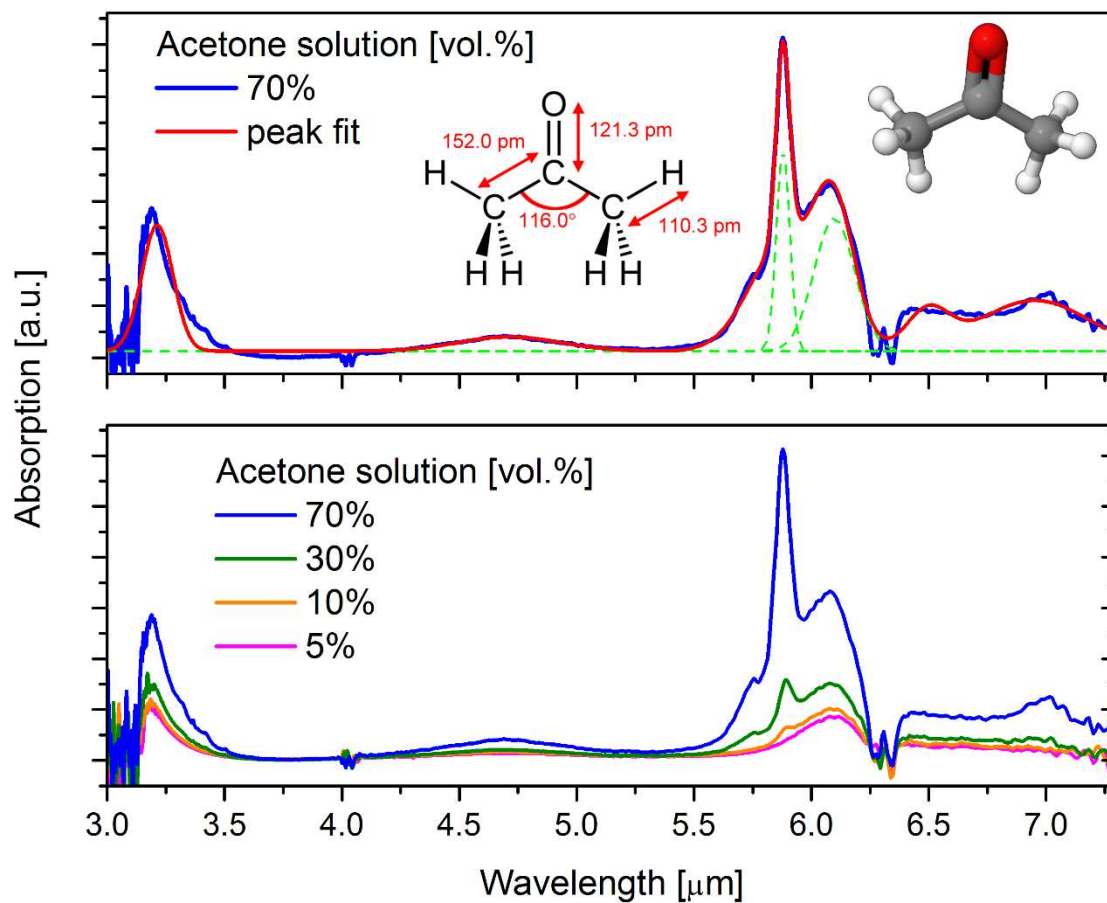
Fig. 13 Absorption spectra of acetone solutions with concentration ranging from 5 to 70 vol.%. The upper figure shows the peak fit for the spectrum (the inset figures show the structural formula and ball-and-stick model). The green dash lines present the fitted peaks, Guassian shape assumed.
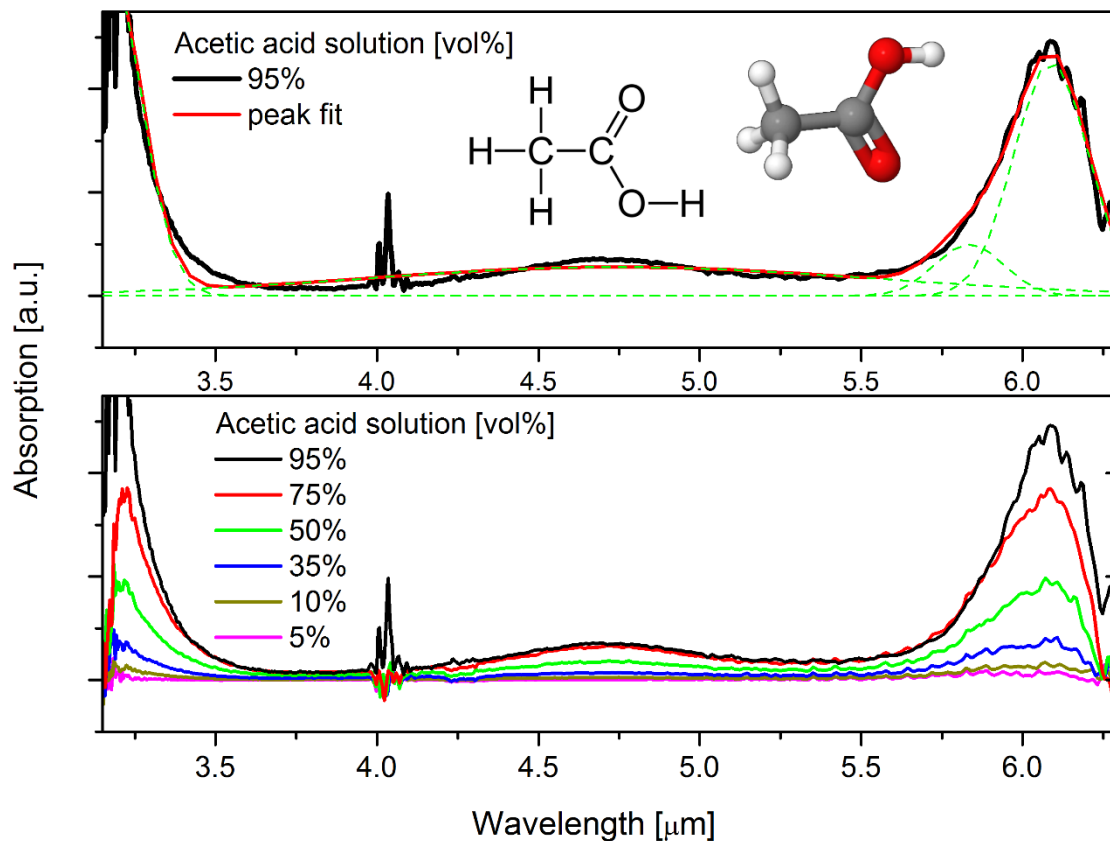
Fig. 14 Absorption spectra of acetic acid solutions with concentration ranging from 5 to 95 vol.%. The upper figure shows the peak fit for the spectrum (the inset figures show the structural formula and ball-and-stick model). The green dash line represents the fitted peaks, Guassian shape assumed.
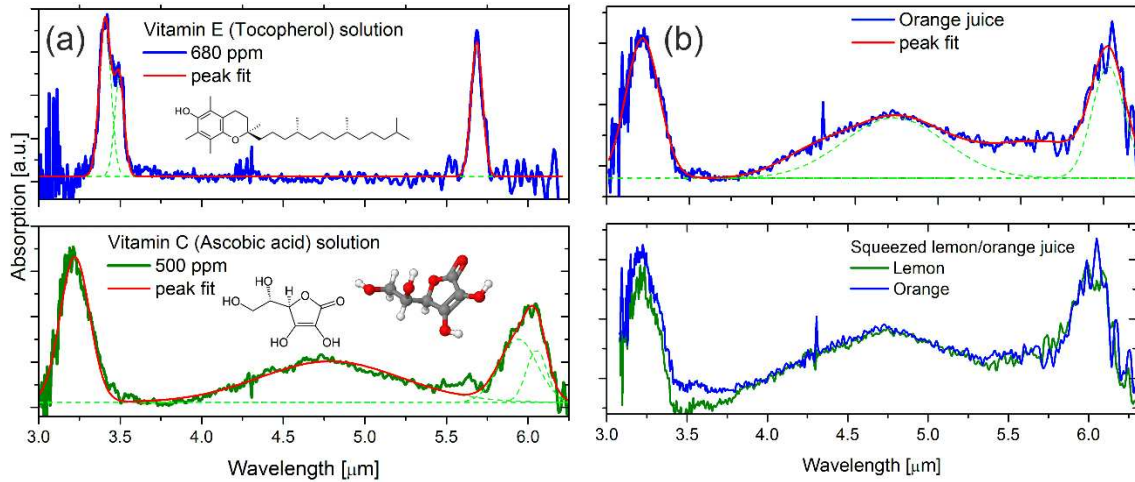
Fig. 15 (a) Absorption spectra of vitamin E and vitamin C solutions in 680 ppm and 500 ppm, respectively (the inset figures show the structural formula and ball-and-stick models). (b) Absorption spectra of squeezed fresh lemon and orange juice. The green dash lines present the fitted peaks, Guassian shape assumed.

Table 1: Typical impurities and absorption bands in chalcogenide glasses and fibres [21-25]

Impurity	Absorption wavelength [μm]
S-H	2.05, 2.54, 3.11, 3.65, 3.94
Se-H	2.32, 3.55, 4.15, 4.57, 5.0
O-H	1.44, 2.2, 2.9, 4.4
Free H_2O	2.77, 2.83, 6.32
Ge-H	4.95
As-H	5.02
Ge-O	7.9, 12.8
P-O	8.3
Se-O	10.67, 11.1, 15.3
Te-O	13.8, 14.4
CO_2	4.31, 4.33, 15.0

Table 2 A comparison of the impurity absorption in purified/un-purified Ge-Te-Se glasses with reported work [21-25].

Absorption	Positions of absorption peak (µm)			Absorption intensity (cm^{-1})		
	This work		Reported work	This work		Reported work
	Un-purified	Purified		Un-purified	Purified	
O-H	2.86	-	2.9	Strong, 1.19	-	Strong
H$_2$O	6.32	-	6.32	Weak, 0.21	-	Medium
Se-H	-	4.52	4.57	Very weak, 0.06	Weak, 0.50	-
Ge-O	7.84, *	-	7.9, 12.8	Strong, 1.73	-	Medium, Strong
Se-O	*	-	11.1,15.3	Strong, 2.13	-	Medium
Te-O	*, 14.74	-	13.8, 14.4	Medium, 1.30	-	Medium
CO/CO$_2$	4.24, 4.30	4.28	4.31	Very weak, 0.14, 0.15	Weak, 0.24	-

* The combination of absorptions from Ge-O, Se-O and Te-O in the un-purified Ge-Te-Se glass contributes to a strong and broad absorption band from 9.4 to 14.4 µm. Therefore, the absorption peaks cannot be identified individually.

Table 3 Effective mode indices from the finite-element calculation

Mode	LP$_{01}$	LP$_{21}$	LP$_{12}$	LP$_{02}$	LP$_{13}$	LP$_{03}$	LP$_{81}$
Refractive index	2.9199	2.9197	2.9195	2.9194	2.9187	2.9182	2.9174

Table 4 Characteristic absorption peaks of chemical species: measured by the FEWS sensor in this paper

Chemical species	Infrared absorption peaks [µm]			
Ethanol	3.362	3.401	3.472	3.535
Methanol	3.115	3.398	3.536	
Acetone	3.177	4.681	5.868	6.091
Acetic acid	3.221	4.765	5.837	6.066
Tocopherol (Vitamin E)	3.418	3.473	5.692	
Ascorbic acid (Vitamin C)	3.183	4.752	5.901	6.031